More hurricanes to hit Western Europe due to global warming

Reindert J. Haarsma, Wilco Hazeleger, Camiel Severijns, Hylke de Vries, Andreas Sterl, Richard Bintanja, Geert Jan van Oldenborgh, Henk W. van den Brink

Royal Netherlands Meteorological Institute (KNMI)

P.O. Box 201, 3730 AE De Bilt, The Netherlands.

haarsma@knmi.nl

Key words: Climate, Hurricanes, Global warming

Abstract

We use a very high resolution global climate model (~25 km grid size) with prescribed sea surface temperatures to show that greenhouse warming enhances the occurrence of hurricane-force (> 32.6 m s^{-1}) storms over Western Europe during early autumn (Aug-Oct), the majority of which originate as a tropical cyclone. The rise in Atlantic tropical SSTs extends eastwards the breeding ground of tropical cyclones, yielding more frequent and intense hurricanes following pathways directed towards Europe. En route they transform into extra-tropical depressions and re-intensify after merging with the mid-latitude baroclinic unstable flow. Our model simulations clearly show that future tropical cyclones are more prone to hit Western Europe, and do so earlier in the season, thereby increasing the frequency and impact of hurricane force winds.

Primary index term: 1630

Other index terms: 1637, 1605, 1626, 1620

1. Introduction

Severe hurricane force (> 32.6 m s^{-1}) storms can cause floods in West-European coastal regions and inflict large-scale damage of infrastructure and agriculture [*Dorland et al.,* 1999; *Sterl et al.,* 2009]. In the present climate, such storms primarily occur in winter and are associated with mid-latitude baroclinic instability. However, global warming and increased sea surface temperatures (SSTs) have the potential to alter the intensity and cause of West-European storms.

In the present-day climate, the vast majority of West-European storms originate from baroclinic instability in the mid-latitudes, which is driven by the north-south atmospheric temperature gradient. In a warmer climate, due to increased concentrations of greenhouse gases, this meridional temperature gradient will decrease because the Arctic will warm faster than the equatorial regions, implying that baroclinic instability will reduce [*Gitelman et al.,* 1997]. In itself this would result in reduced wintertime storms (in frequency and intensity). This is, however, counteracted by the increase of tropopause height and increased latent heat release which tend to intensify storms [*Lorenz and DeWeaver,* 2007]. Recent studies suggest that these two opposing effects may approximately balance, as it has been found that global warming only induces minor changes in the frequency and intensity of mid-latitude storms [*Lambert and Fyfe,* 2006; *Bengtsson et al.,* 2006; *Bengtsson et al.,* 2009; *Leckebusch and Ulbrich*, 2004; *Loptien et al.,* 2008; *Ulbrich et al.,* 2008]. On the other hand, greenhouse warming will result in rising SSTs, which will extend the breeding ground of tropical hurricanes. Recent research indeed suggests that climate warming causes a poleward and eastward extension of the hurricane genesis area [*Zhao and Held,* 2012; *Murakami et al.,* 2012]. This implies

that future hurricanes would be increasingly able to affect extreme mid-latitude storm conditions. As a result, the likelihood of strong storms hitting Western Europe could become larger. Generally, climate warming may thus result in changes in the frequency, intensity and seasonality of Western European storms, for which tropical conditions may become increasingly responsible.

To investigate possible changes in the development and pathways of tropical hurricanes in future climates, climate models are required. Unfortunately, the horizontal resolution of most current climate models is too coarse (100 km or more) to accurately simulate relatively small-scale weather systems such as tropical cyclones. Simulations using high-resolution models, however, indicate that the intensity and frequency of small-scale severe weather systems change significantly as a result of global warming. In particular the intensity of tropical cyclones and heavy precipitation events have been projected to increase [*Zhao and Held,* 2012; *Murakami et al.,* 2012; *Knutson et al.,* 2010; *Bender et al.,* 2010]. High-resolution climate models are thus required to adequately address possible changes in the occurrence of intense storms in Western Europe.

Here we investigate the change in the occurrence of severe mid-latitude storms caused by global warming using the global climate model EC-EARTH [*Hazeleger et al.,* 2010] at very high resolution, so as to adequately resolve small-scale extreme weather systems, including tropical cyclones. We simulate beginning and end of 21st century conditions, and compare both to assess the 21st century trends.

2. Model and Experimental set-up

The atmospheric component of EC-EARTH is derived from the European Centre for Medium-Range Weather Forecasts (ECMWF) numerical weather prediction model, which is also used operationally for forecasting tropical cyclones. The resolution in this experiment is T799 L91 (~25 km horizontal resolution, 91 vertical levels), which was the operational resolution at ECMWF from February 2006 to January 2010.

The experiment consisted of two sets of 5-year 6-member ensemble simulations for 2002-2006 (present) and 2094-2098 (future), respectively, resulting in a 30-year data set for each period. In the present simulations the observed greenhouse gases and aerosol concentrations were used, whereas for the future simulations the concentrations were derived from the RCP 4.5 scenario [*Van Vuuren et al.,* 2011]. The SSTs are prescribed as lower boundary conditions. For the present simulations daily SSTs were taken from the NASA data set [*http://www.ncdc.noaa.gov/oa/climate/research/sst/oi-daily.php*] for the indicated period on a 0.25 degree horizontal resolution. Future SSTs were computed by adding to the present SST field the ensemble mean change in SST as simulated by the ECHAM5/MPI-OM model used in the ESSENCE project [*Sterl et al.,* 2008]. This project consisted of a 17-member ensemble under the SRES A1B scenario, which is compatible with the RCP4.5 scenario. The increase in the global mean temperature at the end of the 21st century is in RCP4.5 about 1 ºC less than in SRESA1B [*Rogelj et al.,* 2012]. Observed sea-ice coverage was taken for the present simulations. For the future simulations the sea-ice coverage was computed by using a linear regression using the present SST and sea-ice cover fields.

A 10-year spin-up run at low resolution (T159) was made for both the present and the future, followed by a 9-month (from January to October) spin-up run at T799 resolution. The 6-member ensemble was made by taking the atmospheric state of one of the first 6 days of October as initial state for each member. Thereafter the model was run for another 3-months until January 1st before the data was used for the analysis. After this spin-up the spread in the atmospheric states was sufficient to treat the 6 runs as independent members.

The choice of the specific years for the present and future period was motivated by the inclusion of dominant modes of variability like El-Niño for the present period and a separation of a multiple of 4 years between present and future for obtaining the same number of leap years in the present and future period.

The storms were tracked backward in time by computing the location of the minimum pressure in the preceding time step (3 hr). This computation was done in an area of 3º by 3º surrounding the present location of minimum pressure. Because our aim is to locate the genesis region, the tracking algorithm ended when the intensity of the storm fell below that of a tropical depression (Beaufort 7; 13.9 m s^{-1}).

3. Results

We focus on changes in severe storms characteristics in four regions along the coast of Western Europe (Fig. 1): Norway, North Sea, Western UK and Gulf of Biscay. For each of these regions we determine the frequency distribution of 3-hourly wind speeds at 10 m height. They show that in the North Sea and Gulf of Biscay there is a clear increase in the frequency of severe winds (Beaufort 11-12, > 28.4 m s^{-1}) during autumn (Fig. 2a-d). The signal is less clear for Norway and the Western UK. Additionally, the season of highest occurrence shifts from winter to autumn in the North Sea and Gulf of Biscay regions. The maximum wind speed in early autumn increases substantially along the Western European coast (Fig. 2e), emphasizing the intensification of extreme winds during that season.

The occurrence of extreme wind speeds can be attributed to a few storms during the 30-year integration period (Fig. 2f). Summed over Norway, the North Sea and the Gulf of Biscay the number of hurricane force storms (Beaufort 12, > 32.6 m s^{-1}) in early autumn (Aug-Oct) increases from 2 to 13 over the 21st century. We have traced back the origin of these events (see Model and Experimental set-up), showing that virtually all future West-European hurricane-force storms originate as hurricanes or tropical storms in the Tropics (Fig. 3b). In contrast, the few hurricane-force storms in the present climate have predominantly an extra-tropical origin (Fig. 3a). This suggests that the climatological mechanisms driving Western Europe hurricane-force winds are likely to change dramatically over the 21st century.

In the supplemental material we show that tropical cyclones will increase the probability of present-day extreme events over the North Sea and the Gulf of Biscay with

a factor of 5 and 25 respectively, with far reaching consequences especially for coastal safety.

In the current climate, the main genesis region for hurricanes is confined to the western tropical Atlantic, where SSTs are above the threshold (27 ºC) required for tropical cyclones to develop. (Note that the SST threshold for tropical storm development will be affected by changes in the stability characteristics of the atmosphere, with the projected tropospheric warming hampering tropical cyclone genesis). Future tropical storms that reach Western European coasts (and cause hurricane-force storms) predominantly originate from the eastern part of the Tropical Atlantic (east of 50 ºW; Fig. 3b). This is because climate warming in the eastern tropical Atlantic causes SSTs to rise well above the 27 ºC threshold (Fig. 3b). The occurrence of hurricane-force winds indeed shows that, notwithstanding the increased atmospheric stability, the eastern boundary of the hurricane development region shifts about 10 degrees to the east in response to the SST rise (Fig. 3c and d). The present development region exhibits a decrease in hurricane frequency (Fig. S1e, supplemental material), which, incidentally, has significant implications for hurricanes reaching North America. This agrees with the finding that the number of Atlantic hurricanes to make landfall in North America is reduced during years with an anomalous warm tropical Atlantic and consequent eastward extension of the development region [*Wang et al.,* 2011].

After their formation, tropical cyclones are being pushed poleward by the beta-effect [*Rossby,* 1948]. Combined with the ambient prevailing westward trade winds this causes the initial path of Atlantic tropical cyclones to be in northwesterly direction. When they reach the mid-latitudes they are caught by the predominant westerly winds, thereby

veering their track in north-easterly direction, with the possibility of reaching Western Europe. Geometrically, this likelihood increases if their genesis region in the tropical Atlantic is further to the east. In addition, the shorter travel distance in the mid-latitudes will enable the 'tropical' characteristics of hurricanes to be better preserved along their journey to Western Europe. Hence, the likelihood of these storms maintaining their strength when reaching Western Europe will increase, as there is simply less time for them to dissipate [*Hart and Evans,* 2001].

The number and strength of hurricanes forming and reaching the mid-latitudes is affected by many factors. An important one is vertical wind shear, associated with differences in SST between the Pacific and Atlantic oceans. In our simulations the change in vertical shear between upper and lower troposphere over the Atlantic basin is small, generally less than 2 m s^{-1} (Fig. 3e), and is not likely to strongly affect the life cycle of hurricanes. Although there is large uncertainty about the wind shear and other factors that affect the genesis and development of hurricanes, our results for the change in frequency and intensity of hurricanes (Fig. S1, supplemental material) are compatible with other studies [*Knutson et al.,* 2010].

Before reaching the Western European coastal regions the tropical storms undergo extra-tropical transition [*Jones et al.,* 2003; *Hart and Evans,* 2001]. Their evolution can be depicted using the cyclone phase space diagrams of Hart [2003]. Figure 4 shows the ensemble mean evolution of the Western Europe hurricane-force storms with tropical origin. Positive (negative) values of –VLT and –VUT indicate a warm (cold) lower and upper core, respectively. For a tropical symmetrical cyclone B is approximately zero, whereas an asymmetrical developing cyclone has a large positive value of B. For details

of the computation of these variables see Hart [2003] and the supplemental material. Tropical cyclones have a warm core and an axial symmetric structure. During extra-tropical transition these typical characteristics disappear [*Hart,* 2003]: the horizontal size of the storm increases, they become asymmetrical, and the core temperature decreases (Fig. 4). Significantly, though, these transformed storms intensify again, but only after they merge with an unstable background flow. In their final stage, one day before hitting Western Europe, they exhibit a rapid and strong intensification (reddish points in Fig. 4). The average MSLP drops from 970 to 952 hPa and the average maximum wind speeds increases from 27 ms^{-1} (Bf 10) to 33.9 ms^{-1} (Bf 12). This is accompanied by a renewed warming of especially the lower part of the core, indicating that diabatic heating due to the release of latent heat plays a crucial role. The anomalously large moisture content of these storms of tropical origin and the increased mid-latitude humidity caused by global warming thus appear to be crucial in their re-intensification. Figures S2 and S3 show a telling example of a re-intensifying storm, its merging with the mid-latitude baroclinic unstable flow, and the re-emergence of its tropical storm characteristics.

For the current climate, the model simulates 18.3 hurricane days (HD) (> 32.6 m s^{-1}), per season which is slightly less than the observed long term mean of 23.8 [*Gray and Landsea*, 1992]. The number of simulated intense hurricane days (IHD) (> 49.2 m s^{-1}, Cat 3-5) is 0.7, much smaller than the observed long term mean of 5.7, illustrating the inability of the model to simulate the most severe hurricanes. The model simulations depict a more than 4-fold increase in major hurricanes over the 21st century, with IHD increasing to 3.1 (See also Fig. S1). More intense hurricanes are generally able to survive longer in a non-supportive environment [*Hart and Evans,* 2001]. The

consequence of the underestimation of IHD in the present climate is that even more hurricanes could hit Western Europe, but higher resolutions would be required to properly investigate this.

Another caveat is that the model uses fixed SSTs, which prevents the possibility of negative feedbacks on intensity due to SST cooling associated with vertical ocean mixing or latent heat fluxes, which might significantly reduce the intensity of hurricanes.

The results of this study are based on two samples of 30 years. Although we argue that the main conclusions are not affected by the small sample size, we realize that more extended simulations are needed to further test our results.

4. Conclusions

We have shown that in our model simulations global warming yields an eastward extension of the development region of tropical storms. Together with higher SSTs this implies that tropical storms are more likely to reach the mid-latitude baroclinic region before they dissipate. After merging with the baroclinic unstable flow in the mid-latitudes they re-intensify, aided by upper-level diabatic heating owing to the release of latent heat. As a result, the re-intensified storm is likely to regain hurricane-force winds along the coast of Western Europe. Such revived hurricanes are known to cause widespread damage along the North American east coast in the current climate. Our model simulations suggest that tropical hurricanes might become a serious threat for Western Europe in the future. Hence, we anticipate an increase in severe storms of predominantly tropical origin reaching Western Europe as part of 21st global warming.

References

Bender M.A.and co-authors (2010), Modeled impact of anthropogenic warming of the frequency of intense Atlantic hurricanes, *Science, 327,* 454-458.

Bengtsson, L., K. I. Hodges, and E. Roeckner (2006), Storm tracks and climate change, *J. Clim., 19***,** 3518–3543.

Bengtsson, L., K. I Hodges, and N. Keenlyside (2009), Will extratropical storms intensify in a warmer climate?, *J. Clim.*, *22,* 2276-2301.

Dorland, C., R. S. J. Tol, and J.P. Palutikof (1999), Vulnerability of the Netherlands and Northwest Europe to storm damage under climate change, *Clim. Change, 43,* 513-535.

Gitelman, A.I., J.S. Risbey, R.E. Kass, and R.D. Rosen (1997), Trends in the surface meridional temperature gradient. *Geophys. Res. Lett., 24,* 1243-1246.

Gray, W.M., and C.W. Landsea (1992), African rainfall as a precursor of hurricane-related destruction on the U.S. east coast, *Bull. Amer. Meteor. Soc., 73,* 1352-1364.

Hart, R.E., and J. L. Evans (2001), A climatology of the extratropical transition of Atlantic tropical cyclones, *J. Clim., 14,* 546-564.

Hart, R.E. (2003), A cyclone phase space derived from thermal wind and thermal asymmetry, *Mon. Wea. Rev*., *131,* 585-616.

Hazeleger, W., C. Severijns, T .Semmler, S. Stefanescu, S. Yang, X. Wang, K. Wyser, E. Dutra, R. Bintanja, B. van den Hurk, T. van Noije, F. Selten, and A. Sterl (2010), EC-Earth: A Seamless Earth-System Prediction Approach in Action, *Bull. Amer. Meteor. Soc., 91,* 1357-1363.

Jones, S. C., and co-authors, (2003), The extra-tropical transition of tropical cyclones: Forecast challenges, current understanding and future directions, *Wea. and Forecasting, 18,* 1052-1092.

Knutson, T.R., J. McBride, J. Chan, K. Emanuel, G. Holland, C. Landsea, I. M. Held, J. P. Kossin, A. K. Srivastava, and M. Sugi (2010), Tropical cyclones and climate change, *Nature Geosci., 3,* 157-163.

Lambert, S. J., and J. C. Fyfe (2006), Changes in winter cyclone frequencies and strengths simulated in enhanced greenhouse warming experiments: Results from the models participating in the IPCC diagnostic exercise, *Clim. Dyn., 26,* 713–728.

Leckebusch, G. C., and U. Ulbrich (2004), On the relationship between cyclones and extreme windstorm events over Europe under climate change, *Global Planet. Change, 44,* 181–193.

Loptien, U., O. Zolina, S. Gulev, M. Latif, and V. Soloviov (2008), Cyclone life cycle characteristics over the Northern Hemisphere in coupled GCMs, *Clim. Dyn.*, *31,* 507–532.

Lorenz, D.J. and E.T. DeWeaver (2007), Tropopause height and zonal wind response to global warming in the IPCC scenario integrations. *Journ. Geophys. Res., 112,* D10119, doi:10.1029/2006JD008087

Murakami, H., Y. Wang, H. Yoshimura, R. Mizuta, M. Sugi, E. Shindo, Y. Adachi, S. Yukimoto, M. Hosaka, S. Kusunoki, T. Ose, and A. Kitoh (2012), Future Changes in Tropical Cyclone Activity Projected by the New High-Resolution MRI-AGCM, *J. Clim., 25,* 3237-3260.

Rogelj, J., M. Meinshausen and R. Knutti (2012), Global warming under old and new scenarios using IPCC climate sensitivity range estimates, *Nat. Clim. Change, 2,* 248–253, doi:10.1038/nclimate1385

Rossby, C.G. (1948), On the displacement and intensity changes of atmospheric vortices, *J. Mar. Res. ,7,* 175-196.

Sterl, A., C. Severijns, H. Dijkstra, W. Hazeleger, G. J. van Oldenborgh, M. van den Broeke, G. Burgers, B. van den Hurk, P. J. van Leeuwen, and P. van Velthoven (2008),

When can we expect extremely high surface temperatures?, *Geophys. Res. Lett., 35,* L14703.

Sterl, A., H. van den Brink, H. de Vries, R. J. Haarsma, and E. van Meijgaard (2009), An ensemble study of extreme North Sea storm surges in a changing climate, *Ocean Science, 5,* 369-378.

Ulbrich, U., J. G. Pinto, H. Kupfer, G. C. Leckebusch, T. Spangehl, and M. Reyers (2008), Changing Northern Hemisphere storm tracks in an ensemble of IPCC climate change simulations, *J. Clim.*, *21,* 1669–1679.

van Vuuren, D.P., J. Edmonds, M. Kainuma, K. Riahi, A. Thomson, K. Hibbard, G. C. Hurtt, T. Kram, V. Krey, J. F. Lamarque, T. Masui, M. Meinshausen, N. Nakicenovi, S. J. Smith, and S. K. Rose (2011), The representative concentration pathways: an overview, *Clim. Change, 109,* 5-31.

Wang C., H. Liu, S.-K. Lee, and R. Atlas (2011), Impact of the Atlantic warm pool on United States landfalling hurricanes, *Geophys. Res. Lett*., *38,* L19702.

Zhao, M, and I. M. Held (2012), TC-Permitting GCM Simulations of Hurricane Frequency Response to Sea Surface Temperature Anomalies Projected for the Late-Twenty-First Century, *J. Clim.,* 25, 2995-3009.

Figure Captions

Figure 1. SST (ºC) change between future (2096-2098) and present (2002-2006) for Aug-Oct. The SST change is derived from the ESSENCE model (see Model and Experimental set-up). The colored squares indicate the different analysis regions: Norway (60º-70º N, 0º-15º E) [blue], North Sea (50º-60º N, 3º W-8º E) [red], Western UK (50º-60º N, 3º-15º W) [green], Gulf of Biscay (43º-50º N, 0º-15º E) [light blue].

Figure 2. Wind speed changes over the 21st century along the Western European coast. **a-d,** Frequency distribution of the 3-hourly 10m windspeed (U10) area-averaged over the different analysis regions for Beaufort 11-12 (U10 > 28.4 m s^{-1}) for present (blue) and future (red) conditions. The frequency is multiplied by 10^2. The 95% significance intervals based on a Poisson distribution for the Future peaks in October for North Sea and Biscay are indicated by vertical bars. **e,** Wind speed change (m s^{-1}) for the period (Aug.-Oct.) between future and present conditions. Results are significant at 95% confidence level. Return period computations are done for the location of the black cross (See supplemental material, Fig. S4). **f,** Number of hurricane force storms during (Aug-Oct) in the different basins for the present (blue) and future (red) climates.

Figure 3. Tracks and frequency of hurricane-force storms. Upper panels: backward tracks of storms with Beaufort 12 (> 32.6 m s^{-1}) in one of the four analysis regions of Fig. 1 during early autumn (Aug-Oct) for **a,** present and **b,** future climate. The storm intensity is indicated by the colors of the tracks. The SSTs (ºC) during early autumn (Aug-Oct) for

present and future climates are plotted as background. The black solid line denotes the 27 ºC isotherm. Lower panels: frequency (multiplied by $2x10^4$) of 3-hourly Beaufort 12 (> 32.6 m s^{-1}) wind speeds during (Jul-Oct) for **c,** present and **d,** future climate. The vertical wind shear (m s^{-1}) between 850 and 200 hPa, computed as the length of the difference wind vector between these two levels, is depicted in **e**. Contours: present climate. Shaded: future minus present climate.

Figure 4. Mean evolution of Western Europe hurricane-force storms during the last 6 days before they hit the Western European coast, represented in cyclone phase space **a,** -VLT vs B and **b,** -VLT vs -VUT. A circular marker is placed every 8 h. The numbers next to the markers indicate the days before hitting the Western European coast. The color of the markers indicates the MSLP intensity and the size the mean radius R of the cyclone.

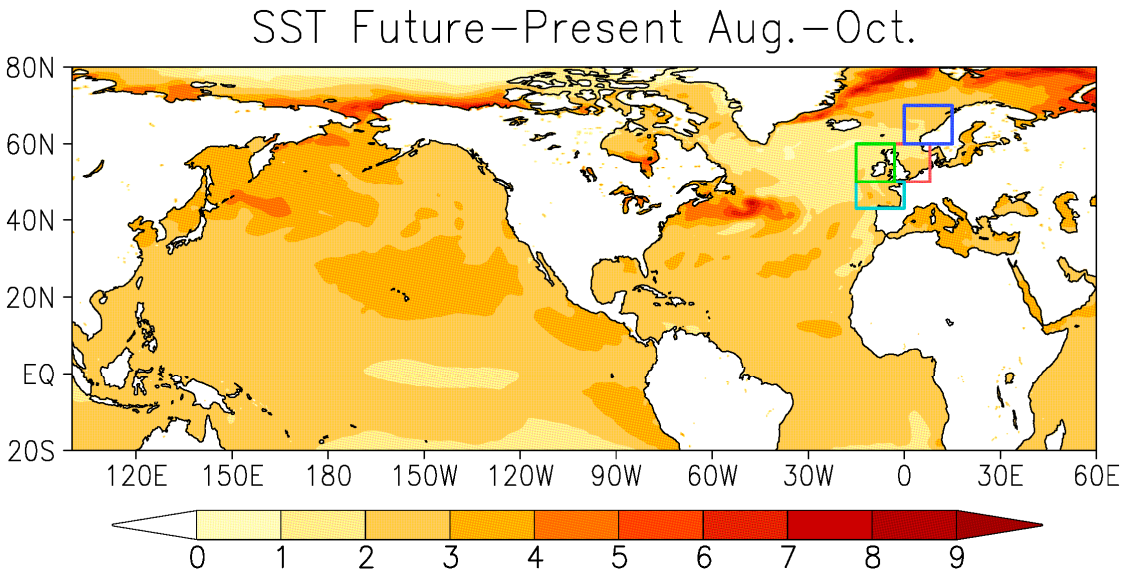
SST Future−Present Aug.−Oct.
80N
60N
40N
20N
EQ
20S
120E
150E
180
150W
120W
90W
60W
30W
0
30E
60E
0
1
2
3
4
5
6
7
8
9

Fig. 1

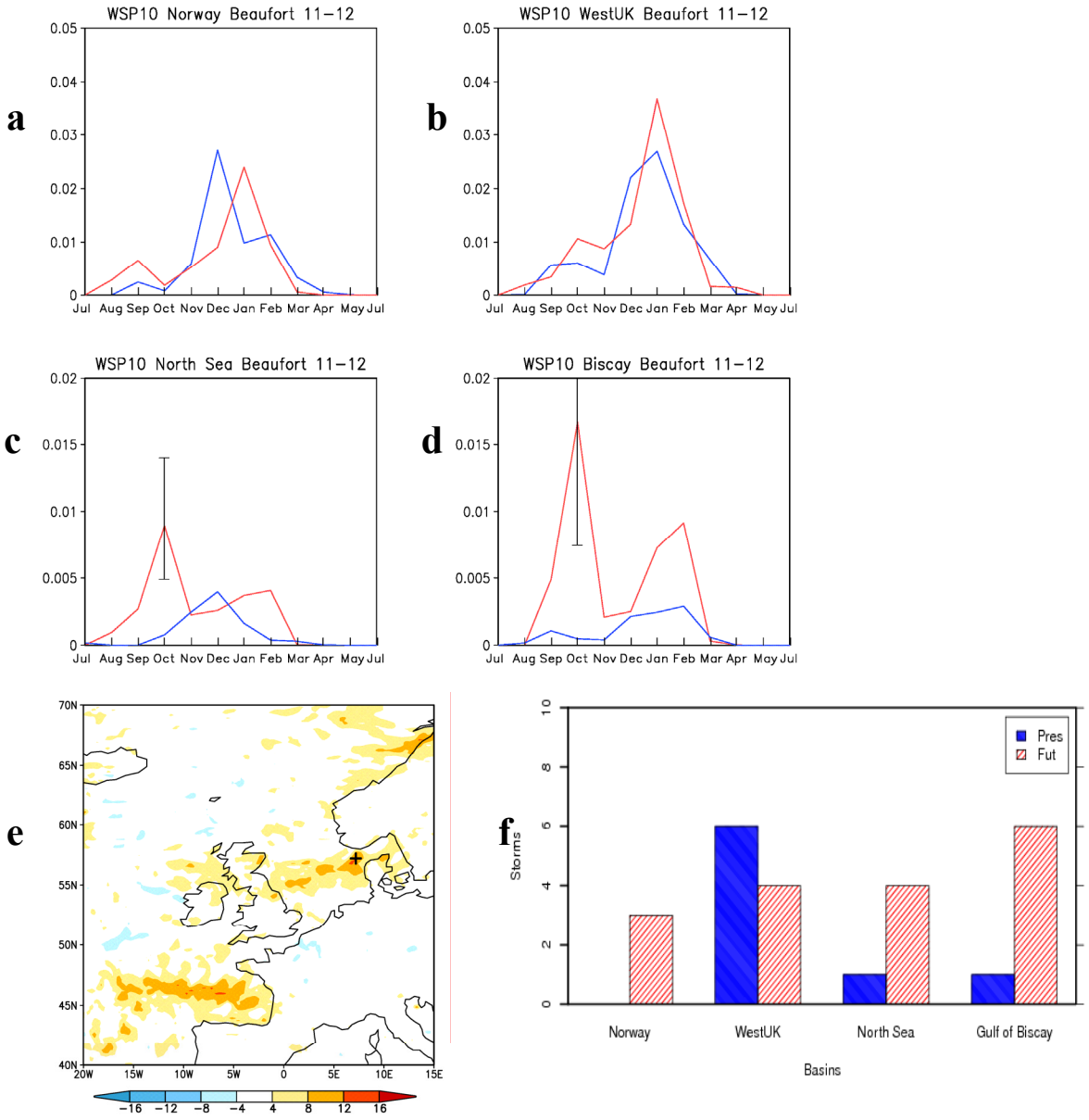
a
WSP10 Norway Beaufort 11–12
b
WSP10 WestUK Beaufort 11–12
c
WSP10 North Sea Beaufort 11–12
d
WSP10 Biscay Beaufort 11–12
Jul Aug Sep Oct Nov Dec Jan Feb Mar Apr May Jul
e
f
Pres
Fut
Storms
Norway
WestUK
North Sea
Gulf of Biscay
Basins

Fig. 2

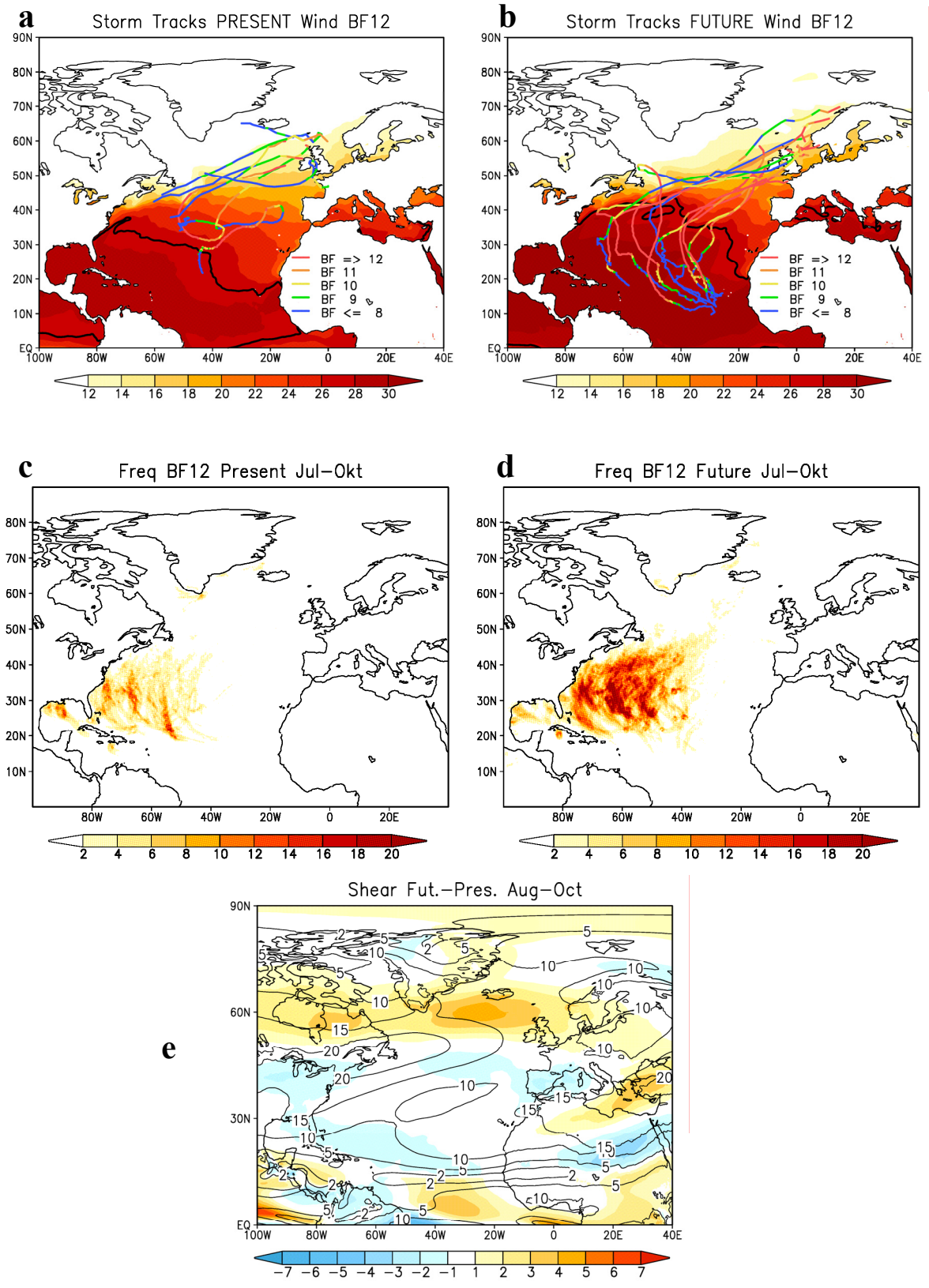
a
Storm Tracks PRESENT Wind BF12
BF => 12
BF 11
BF 10
BF 9
BF <= 8
12 14 16 18 20 22 24 26 28 30
b
Storm Tracks FUTURE Wind BF12
BF => 12
BF 11
BF 10
BF 9
BF <= 8
12 14 16 18 20 22 24 26 28 30
c
Freq BF12 Present Jul–Okt
2 4 6 8 10 12 14 16 18 20
d
Freq BF12 Future Jul–Okt
2 4 6 8 10 12 14 16 18 20
e
Shear Fut.–Pres. Aug–Oct
−7 −6 −5 −4 −3 −2 −1 1 2 3 4 5 6 7

Fig. 3

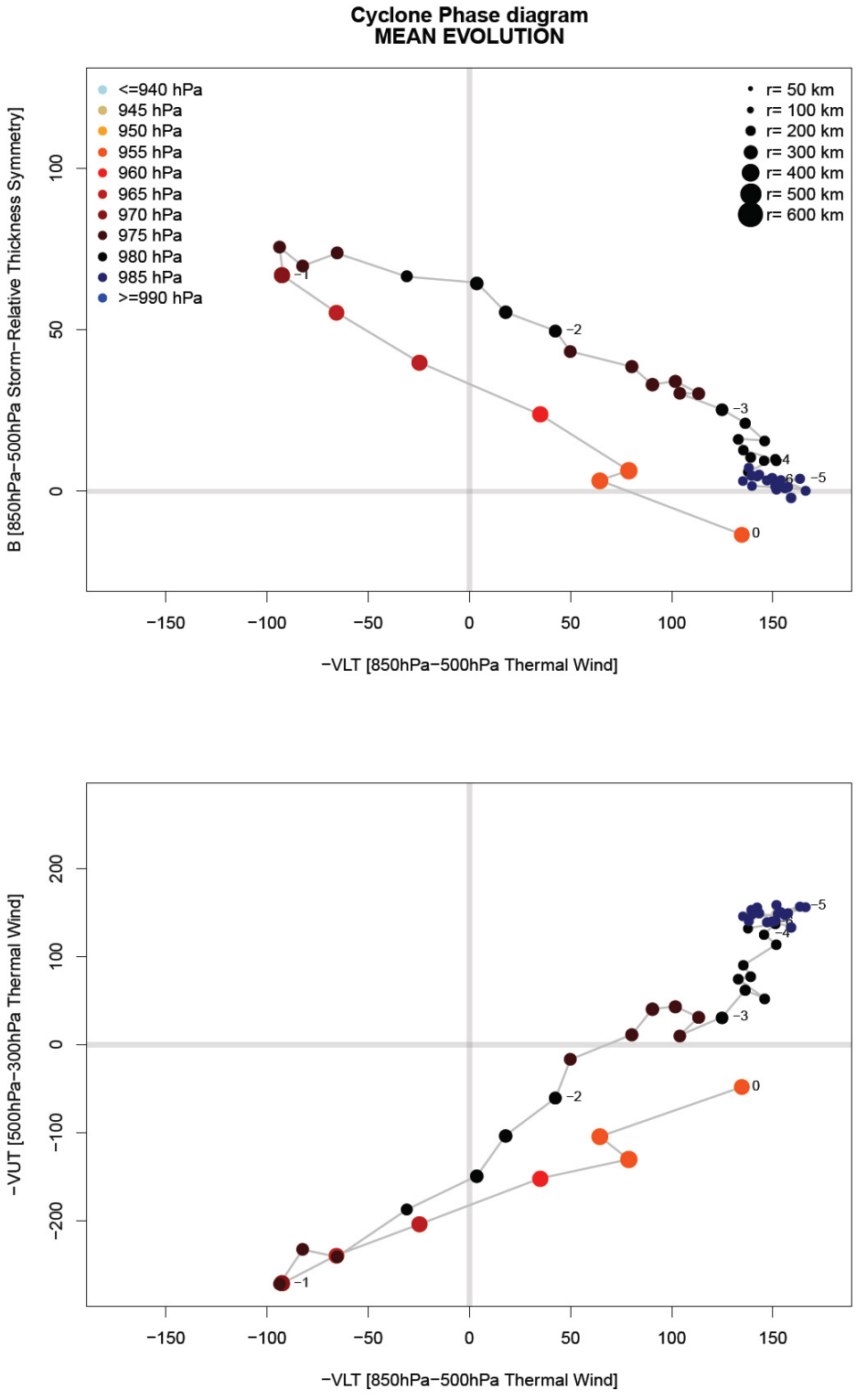
Cyclone Phase diagram
MEAN EVOLUTION
<=940 hPa
945 hPa
950 hPa
955 hPa
960 hPa
965 hPa
970 hPa
975 hPa
980 hPa
985 hPa
>=990 hPa
r= 50 km
r= 100 km
r= 200 km
r= 300 km
r= 400 km
r= 500 km
r= 600 km
B [850hPa−500hPa Storm−Relative Thickness Symmetry]
−VLT [850hPa−500hPa Thermal Wind]
−VUT [500hPa−300hPa Thermal Wind]
−VLT [850hPa−500hPa Thermal Wind]

Fig. 4

Supplemental Material

The supplemental material contains additional analyses, figures, and a description of the storm characteristics as used in the phase diagrams of Hart [2003]. The additional analyses include a potential vorticity analysis of a merging hurricane and a return period analysis of maximum wind speeds.

Storm characteristics

For the computation of the evolution of the storm characteristics we use the phase diagrams of Hart [2003] and Evans and Hart [2003]. In these diagrams the time evolution of the following quantities is displayed.

- Storm-motion-relative 850-500 hPa thickness asymmetry, across the cyclone within 500 km radius , B:

$$B = h(\overline{Z_{500hPa} - Z_{850hPa}}\,|_R - \overline{Z_{500hPa} - Z_{850hP}}\,|_L),$$

where Z is isobaric height, R indicates area to the right of current storm motion, L indicates area to the left of storm motion and the overbar indicates the areal mean over a semicircle of radius 500 km. The integer h is +1 for the Northern Hemisphere and -1 for the Southern Hemisphere.

B indicates the frontal nature of the storm. For tropical cyclones it is approximately zero, while a developing large extra-tropical cyclone has a large positive value of B. The threshold value between tropical and extra-tropical cyclones is about 10.

- Characteristics op upper and lower core. Upper and lower troposphere thermal wind: -VUT and –VLT:

$$-VUT = \frac{\partial(\Delta Z)}{\partial \ln p}\Big|_{500hPa}^{300hPa}, \quad -VLT = \frac{\partial(\Delta Z)}{\partial \ln p}\Big|_{850hPa}^{500hPa},$$

where $\Delta Z = Z_{max} - Z_{\min}$ is the cyclone perturbation of the geopotential, which is evaluated in the 5º by 5º grid box surrounding the center of the storm indicated by its minimum MSLP.
Storms with positive (negative) values of -VUT (-VLT) have a warm (cold) upper (lower) core .

- Radius of the storm, R.

R is computed as the mean radius of 10-m gale force (17.5 ms^{-1}) wind speed.

- Minimum mean sea level pressure (MSLP) of the storm.

Return periods

We illustrate the dramatic changes in the Western European extreme-wind climate due to tropical cyclones for a grid point on the North Sea (7.2 ºE, 57.2 ºN) by a Gumbel plot, as shown in Figure S4. This graph shows the 30 wind maxima for Augustus-October as a function of the estimated return period for the future climate as well as the estimated Gumbel distributions [*Coles,* 2001; *van den Brink and Können,* 2008]. The winds due to the tropical cyclone (occurring on October 7 2097 of member 5) are by far the highest in the 30 years (37 m s^{-1}). According to a Gumbel fit to all 30 maxima, this event corresponds to a return period of more than 20,000 years.

In order to investigate for how many gridpoints situations as shown in Figure S4 occur, Figure S5 shows the histogram of the estimated return periods of the 30-year maximum based on all (~2000) gridpoints per box. The blue line shows the distribution of all estimated return periods for the present climate in the box-area, and the red one for the future climate. It shows that for the current climate, most grid points have a maximum with a return period around 30 years, which is as expected for 30-year records. It also shows that the frequency of events with high return periods (> 100 years) is about 5, 10 and 25 times higher for future than for present-day events for the North Sea, Norway and Biscay area, respectively, whereas West UK shows a slight decrease in the frequency of

events with high return periods.

The considerable increase in the frequency of extreme events will have far reaching consequences for in particular coastal defense. As an example, the dike design criteria for The Netherlands are based on the 10,000-year return levels, which may be considerably higher in the future climate.

References

Coles. S. (2009), An introduction to statistical modeling of extreme values, *Springer-Verlag,* ISBN 1-85233-459-2.

Evans, J. I., and R.E.A. Hart (2003), Objective indicators of the life cycle evolution of extra-tropical transition for Atlantic tropical cyclones. *Mon. Wea. Rev., 131,* 909-925.

Hart, R.E. A (2003), Cyclone phase space derived from thermal wind and thermal asymmetry. *Mon. Wea. Rev., 131,* 585-616.

van den Brink, H. W., and G. P. Können (2008), The statistical distribution of meteorological outliers, *Geophys. Res. Lett., 35,* L23702, doi:10.1029/2008GL035967.

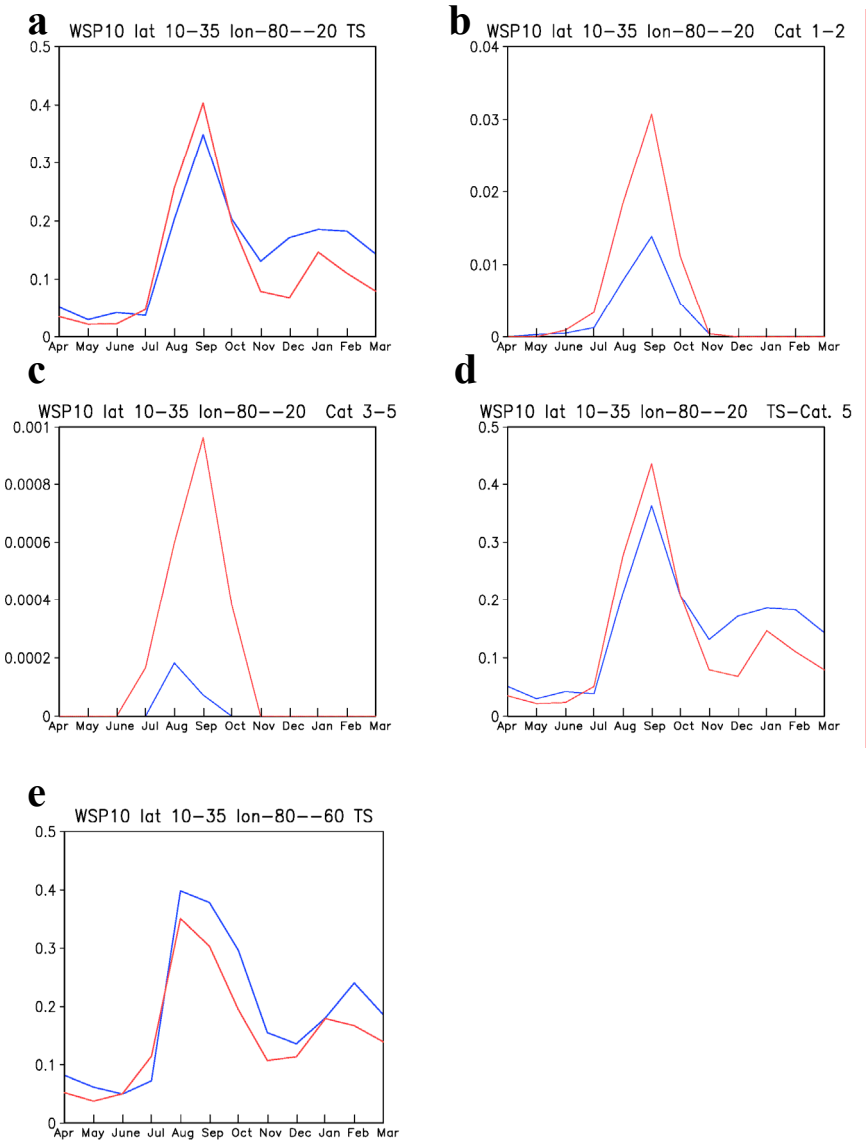

Figure S1. Wind speed frequency in tropical Atlantic. **a-d,** Frequency distribution of wind speed at 10 m of tropical storm strength in the tropical Atlantic area-averaged over the region (10º-35º N, 80º-20º W). **a,** Tropical storms (17.5-32.6 m s^{-1}), **b,** Category 1-2 hurricanes (32.6-49.2 m s^{-1}), **c,** Category 3-5 hurricanes (> 49.2 m s^{-1}). **d,** All tropical storms (> 17.5 m s^{-1}). **e,** Same as **a** but now area-averaged over the region (10º-35º N, 80º-60º W). Blue: present. Red: future. The frequency is multiplied by 10^2.

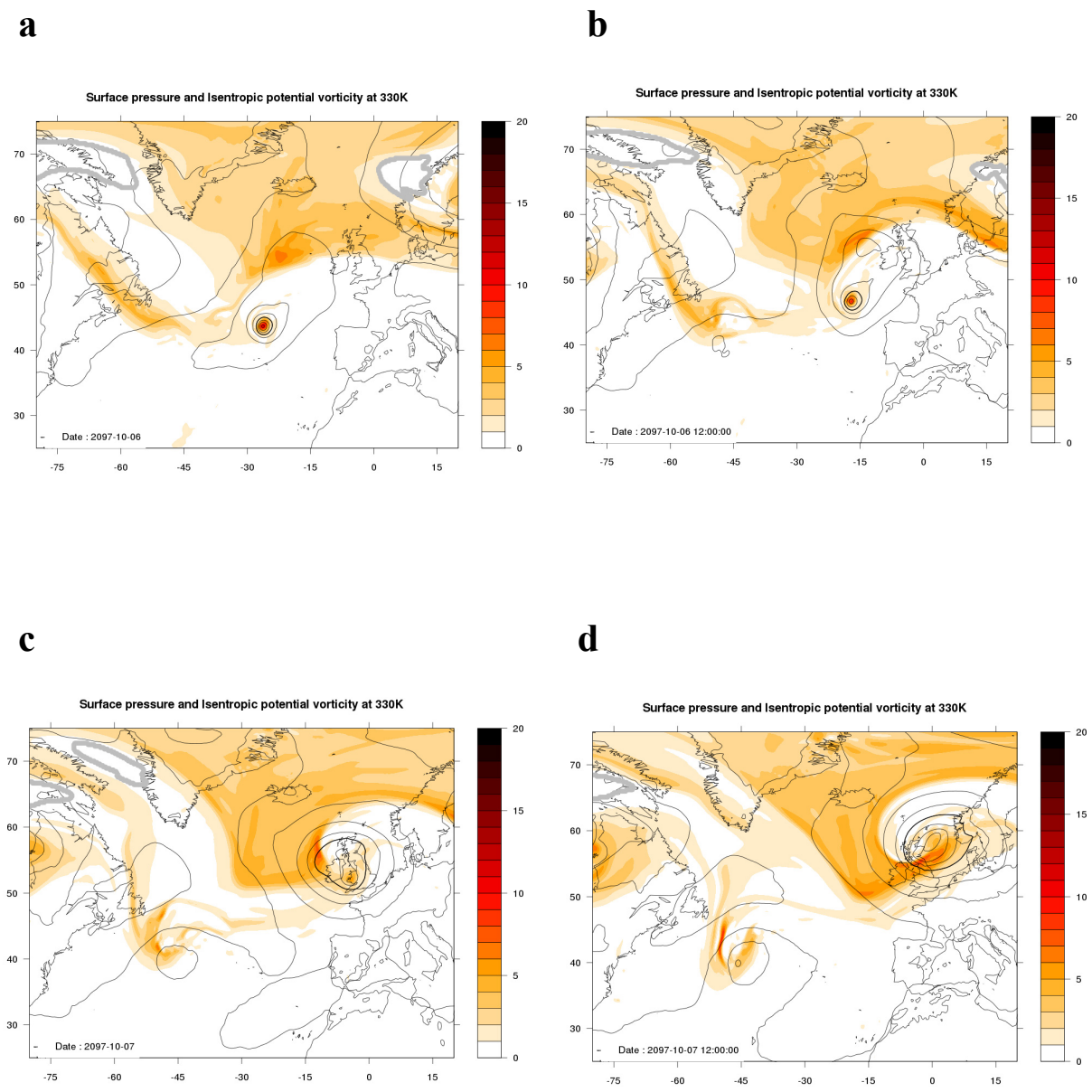

Figure S2. Merging of tropical cyclone with the mid-latitude background flow. **a-d,** Example of the merging of a tropical cyclone with a baroclinic unstable flow and its subsequent intensification. Contours: mean sea level pressure MSLP (hPa). Contour interval: 10 hPa. Thick contour: 980 hPa. Arrows: 10 m windspeed (m s^{-1}). Shaded: potential vorticity (PV) in potential vorticity units (PVU) on the 320K isentropic surface. The time interval between the different plots is 12 hr.

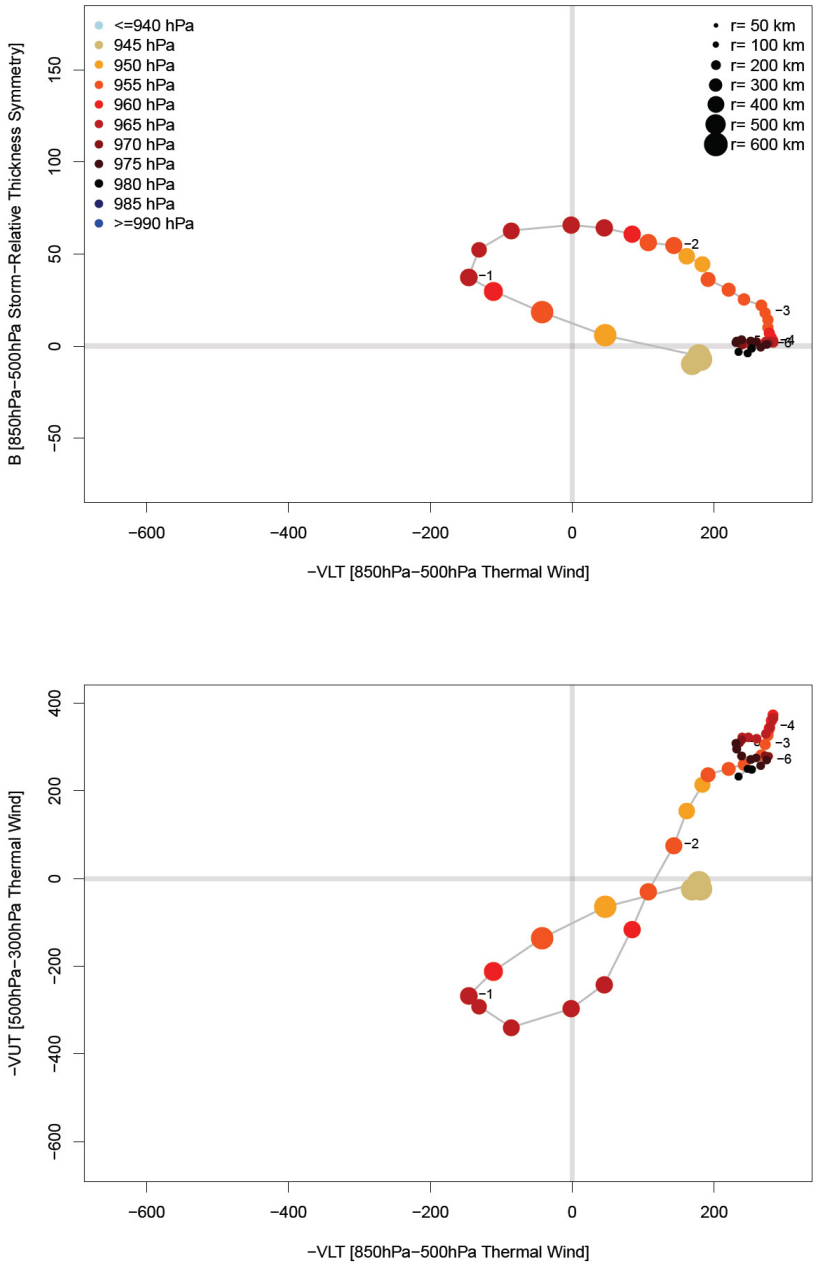

Figure S3. Evolution of the storm in Fig. S2 during its last 6 days before it hits the Western European coast, represented within cyclone phase space **a,** -VLT vs B and **b,** -VLT vs -VUT. A circular marker is placed every 6 h. The numbers next to the markers indicate the days before hitting the Western European coast. The color of the markers indicates the MSLP intensity and the size the mean radius R of the cyclone.

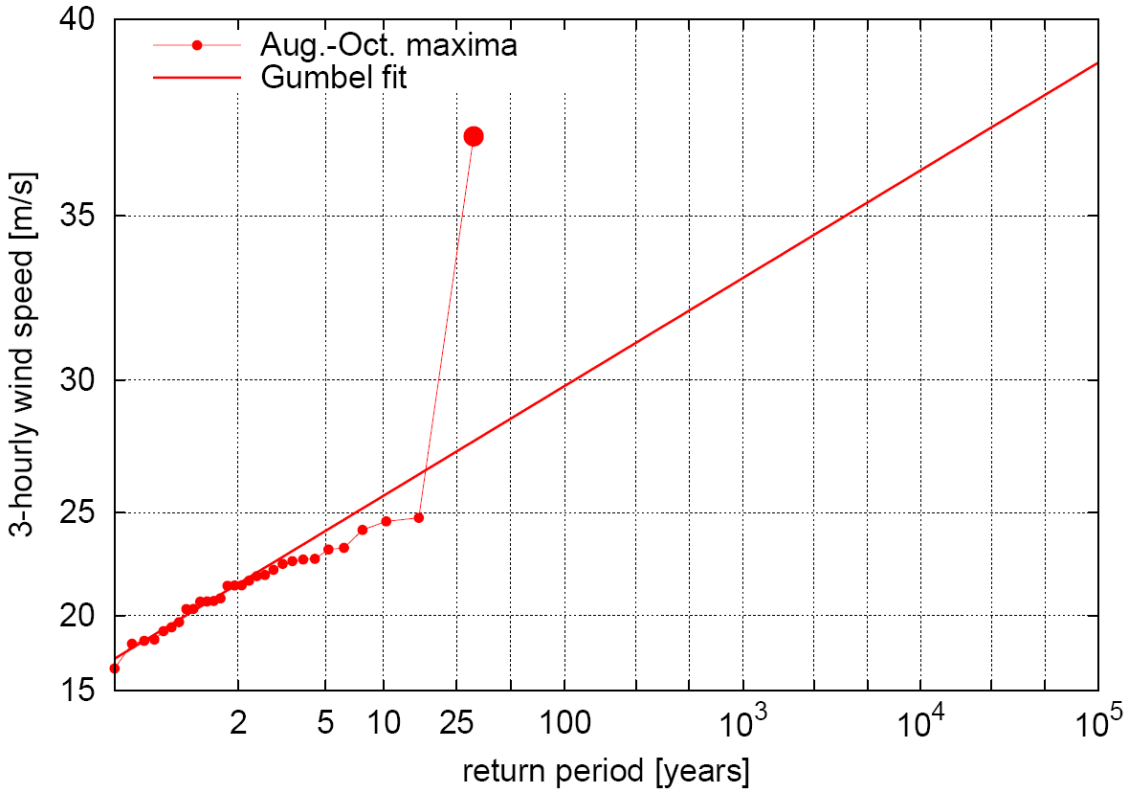

Figure S4. Gumbel plot of the future 3-hourly 10m wind speed maxima for Aug.-Oct. at (7.2 ºE, 57.2 ºN) (indicated by a black cross in Fig. 2e). According to the fit (red line) the outlier (large red dot, occurring on October 7 2097 of member 5) has an estimated return period of more than 20,000 years.

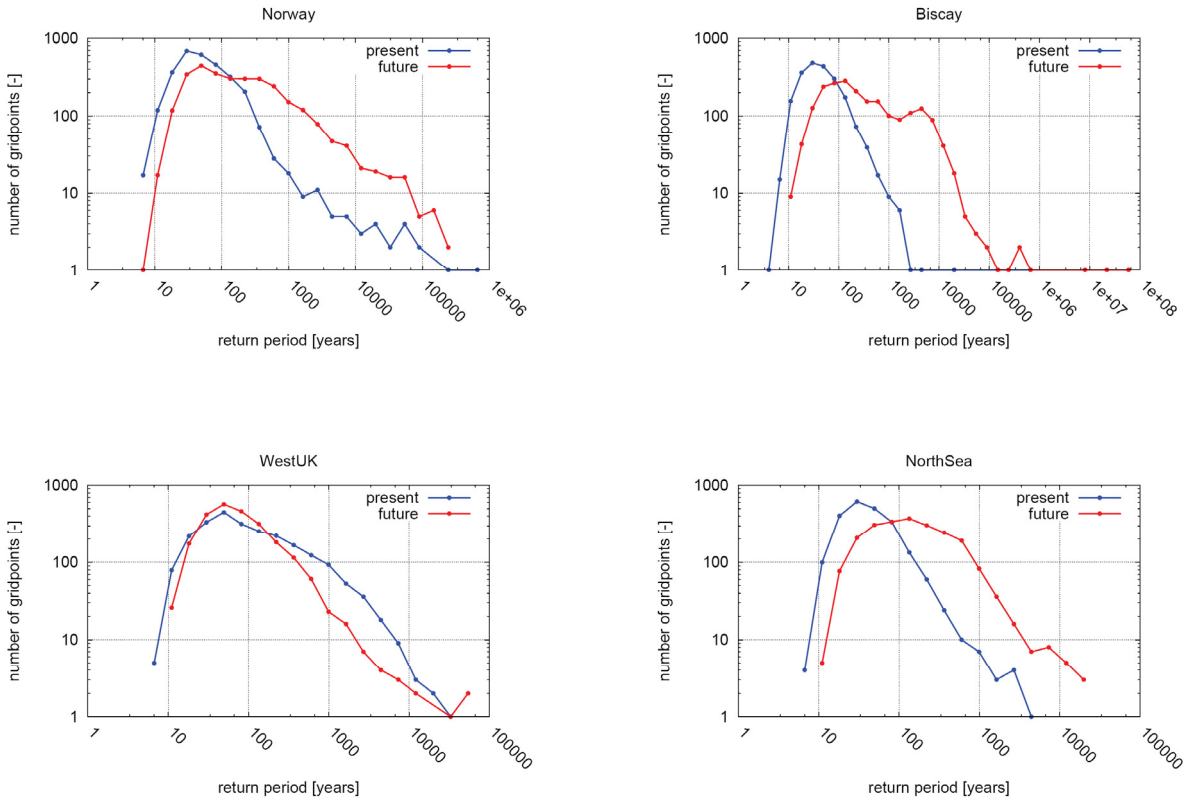

Figure S5. Histograms for the 4 boxes Norway, Biscay, WestUK and NorthSea of the estimated return periods for the highest wind speed per grid point. The blue line represents the distribution of return periods for the present climate, the red one for the future climate. The number of grid points per box varies between 2077 and 2385.